energies

MDPI

*Article*

# An Analysis of Misalignment Resilience and Interoperable Characteristics of the Segmented Bipolar Pad for Wireless EV Charging System

**Bharathi Manivannan [1], Balasubramanian Ramalingam [1], Parkavi Kathirvelu [1,*], Natarajan Prabaharan [1,*], Mohammad Alhuyi Nazari [2,3,*] and Mohamed Salem [4,5,6]**

1 School of Electrical & Electronics Engineering, SASTRA Deemed University, Thanjavur 613401, India; bharathi1315@gmail.com (B.M.); rbalu@eee.sastra.edu (B.R.)
2 Engineering School, Department of Mechanical Engineering, Central Asian University, Tashkent 111221, Uzbekistan
3 Faculty of New Sciences and Technologies, University of Tehran, Tehran 1417935840, Iran
4 Institute of Research and Development, Duy Tan University, Da Nang 550000, Vietnam; mohamadsalemmohamedothman@duytan.edu.vn
5 School of Engineering & Technology, Duy Tan University, Da Nang 550000, Vietnam
6 School of Electrical and Electronic Engineering, Universiti Sains Malaysia (USM), Nibong Tebal 14300, Penang, Malaysia
* Correspondence: to_parkavi@eee.sastra.edu (P.K.K.); prabaharan.nataraj@gmail.com (N.P.); m.alireza@centralasian.uz (M.A.N.)

**Abstract**

This paper proposes a novel magnetic coupler, a segmented bipolar pad (SBP) that outperforms the conventional bipolar pad (BP) with symmetrical geometrical dimensions. The performance parameters: mutual inductance ($M_{TR}$), coupling coefficient ($k$), output power ($P_O$), and DC-DC efficiency ($\eta$). The performance evaluation of the proposed pad is compared with the conventional pad under cases: (1) lateral misalignment (ΔY), and (2) interoperability with non-polarized pad (NPP) and polarized pad (PP). A 4.7 kW inductive power transfer (IPT) system is designed with an inductor–capacitor–capacitor-series (LCC-S) compensation network. For case 1, the $M_{TR}$ of the SBP at ΔY = ±90 mm is the same as the $M_{TR}$ of BP at ΔY = 0 mm, ensuring better misalignment tolerance capability of SBP. The maximum $\eta$ of SBP is 93.64%, which is 4.96% greater than the highest $\eta$ of BP. For case 2, the $M_{TR}$ of the SBP with NPP is 22–24% and with PP is 20–25% higher than the BP interoperable performance. The obtained $\eta$ shows maximum improvement of 2.46% for SBP with NPP, and 3.7% for SBP with PP when compared to the interoperable results of BP. SBP gives enhanced performance for both cases compared to the conventional pad at no additional pad design cost. The proposed work is validated through an experimental setup.

**Keywords:** electric vehicle; segmented bipolar pad; inductive power transfer; misalignment; interoperability



Academic Editor: Ping Lu

Received: 29 December 2025
Revised: 24 February 2026
Accepted: 27 February 2026
Published: 3 March 2026



## 1. Introduction

In recent years, electric vehicles (EVs) have retained their consistent growth in the automotive industry by offering a promising path towards a sustainable environment and cutting down the dependency on fossil fuels [1]. The transition to EV from conventional internal combustion engine (ICE) vehicles is contributing to a cleaner and more sustainable energy future. However, the widespread adoption of electrified transportation relies completely on the convenient and safe charging of EV batteries [2]. Wireless power transfer (WPT), an optimistic technology, is highly entertained by the researchers involved in the field of EV charging enhancement. The WPT technology eliminates the need to handle cables and facilitates automatic and reliable EV powering [3]. Among several methods of WPT technology, the inductive power transfer (IPT) method has been widely applied in industrial sectors, which utilizes the electromagnetic induction principle for achieving high power transmission [4]. A magnetic coupler system consists of a ground-embedded pad called a transmitter (Tx) and a vehicle-fitted pad called a receiver (Rx), combinedly known as charging pads, which are the key elements of IPT technology [5]. The major challenge in EV powering through the IPT concept is designing anti-misalignment magnetic coupler pads. The misalignment between charging pads causes significant flux leakage and a reduced coupling coefficient that pulls down the overall system efficiency [6]. Another research consideration is to improve the interoperable nature of the Tx pad with different Rx pads to accommodate the unique pad design of various EV models [7,8]. It is a crucial part for the designers to address critical issues like misalignment and the interoperability characteristics of magnetic couplers.

Different shapes and designs of coupling pads are proposed by the researchers in an attempt to improve the misalignment tolerance and the interoperability performance rate. In the literature [9], the authors have made a comparative analysis of non-polarized pads (NPP), including circular and square geometrical coils. Further, they studied the performance of the coils with lateral misalignment conditions. Based on the performance comparison, the authors suggested the square coil arrangement as the best one for the WPT application. However, the NPP coils addressed in the above work facilitate only vertical flux components. At the same time, polarized pads (PP) like double-D pad (DDP), double-D quadrature pad (DDQP), and bipolar pad (BP) produce both vertical and horizontal flux components and show better power transmission irrespective of misaligned receiver pads [10]. Mohammad Ibrahim et al. [11] have studied the interoperability performance of three different commercial vehicle models, including Renault, Schneider, and the NewTech inductive pad. An analysis between the rectangular pad (RP) and DDP was conducted, and the performance evaluation was carried out based on parameters such as coupling coefficient, output power, and efficiency [8]. An interoperable characteristic between two NPP, like square and circular, has been studied under different misalignment distances based on the key parameter mutual inductance [12].

In the literature [13], an interoperability analysis is conducted between the quadruple coil as the Tx and different receiver pads, including rectangular, DDP, and DDQP. The compatibility study is based on the evaluation parameters, like mutual inductance between transmitter and receiver pads ($M_{TR}$) and coupling coefficient ($k$) under misalignment. Gautam Rituraj [14] proposed a unipolar coil arrangement method (UCAM) to reduce the leakage flux and improve the power transmission efficiency by achieving the maximum coupling coefficient. The interoperability nature of the proposed UCAM-based coil with the conventional coil is studied. However, the UCAM approach has been conducted only on NPP by varying the number of turns of the rectangular coil of different geometries. In the literature [15], an adaptive position adjustment method is used to improve the interoperable behavior between rectangular and DDP against misalignment conditions. In the literature [16], the authors proposed a coil structure that comprises a pair of DDP placed inside a large rectangular coil. The interoperability of the designed structure is studied for different receiver coils for the application of unmanned aerial vehicle (UAV). Ankur Yadav et al. [17] developed a honeycomb magnetic coupler by modifying the design of the rectangular pad to improve the magnetic coupling of the charging pad. However, these works have not carried out any design modification in the conventional BP with similar geometrical dimensions to study its misalignment tolerance and interoperability characteristics.

Meanwhile, some work has utilized a ferrite core design in the coil to improve the mutual inductance between charging pads [9]. Itay Garrofy et al. [18] proposed multiple coils wound vertically over the ferrite core, unlike the planar DDQP. The vertical receiver coil (VC) shows better transmission efficiency when compared to DDQP. Nevertheless, the addition of the ferrite core to the coil leads to an increase in the system's weight and cost [19]. Considering these limitations, modifying the coil design is the appropriate way to enhance the coupling coefficient ($k$) rather than adding ferrite material. In the literature [20], the authors showed that an improved coupling coefficient can be achieved by minimizing the self-inductance of the coil through optimizing the pad structure. The authors in the literature [21,22] have proposed an intermediate coil design in the square and circular magnetic coupler for achieving a better coupling coefficient between charging pads. However, the works that have been presented so far only deal with unipolar coil structures. The comparison of the proposed coil with the existing works is provided in Table 1.

**Table 1.** Comparison with existing works.

| Ref. | Coil Structure | Coil Size | Symmetrical Geometrical Dimensions to the Conventional Coil | Design Modification in BP | Analysis | | |
|---|---|---|---|---|---|---|---|
| | | | | | Lateral Misalignment | Interoperability | |
| | | | | | | NPP | PP |
| [12] | Square<br>Circular | - | - | ✗ | ✔ | ✔ | ✗ |
| [13] | Quadruple<br>RP<br>DDP<br>DDQP | 200 × 100 mm | ✔ | ✗ | ✔ | ✔ | ✔ |
| [14] | RP | 400 × 300 mm | ✗ | ✗ | ✔ | ✔ | ✗ |
| [15] | RP<br>DDP | 650 × 500 mm<br>650 × 600 mm | ✗ | ✗ | ✔ | ✔ | ✔ |
| [17] | Honeycomb<br>RP | 400 × 400 mm | ✔ | ✗ | ✔ | ✗ | ✗ |
| [18] | VC<br>DDQP | 500 × 500 mm | ✔ | ✗ | ✗ | ✗ | ✗ |
| [23] | Solenoid DD (SDD)<br>DD<br>RP | 320 × 300 mm | ✔ | ✗ | ✔ | ✔ | ✔ |
| Proposed work | SBP<br>BP | 300 × 350 mm | ✔ | ✔ | ✔ | ✔ | ✔ |

It has been noticed from the literature that most of the works have not approached the design modification of the BP structure for improving the mutual inductance and coupling coefficient between transmitter and receiver pads. This work proposes a magnetic coupler SBP, which is developed through a systematic design refinement of conventional BP structures. Partitioning the number of turns of the BP into a new segment to form a quadrature coil is known as the SBP. The SBP outperforms the conventional bipolar pad (BP) with symmetrical geometrical dimensions. The performance of SBP exhibits notably improved mutual inductance and coupling coefficient between Tx and Rx pads. The enhanced magnetic coupling leads to considerably higher output power and DC-DC efficiency of the IPT system. The proposed coil attains improved tolerance to lateral misalignment and better interoperable characteristics with the NPP and PP compared to the BP.

In this context, the main objectives of this article are given below:

1. This paper proposes a novel magnetic coupler structure, segmented bipolar pad (SBP), which has been utilized to develop the anti-misalignment IPT system incorporating inductor–capacitor–capacitor-series (LCC-S) compensation topology for EV charging.
2. The proposed pad has been compared with an existing bipolar pad (BP) designed with identical geometrical dimensions. The comparative analysis has been conducted through a graphical representation of parameters, including mutual inductance between Tx and Rx pads ($M_{TR}$), coupling coefficient ($k$), output power ($P_O$), and DC-DC efficiency ($\eta$). The behaviors of the proposed pad are analyzed at the lateral misalignment ($\Delta$Y) as per the specified tolerance range of SAE J2954 standard given in Table 2 [24].
3. This paper analyzes the interoperability nature of the proposed pad with a non-polarized rectangular pad and a polarized bipolar pad.
4. In addition, the paper furnishes detailed theoretical modeling of the IPT system, incorporating the LCC-S compensation network.

**Table 2.** SAE J2954 specification to the proposed work.

| SAE J2954 Requirement | Specification | Proposed Work |
|---|---|---|
| Power class | WPT 2 (up to 7.7 kW) | 4.7 kW |
| Lateral misalignment tolerance | Up to ±100 mm | ±90 mm |
| Vertical air gap between Tx and Rx | Z1 class (100–150) mm | 100 mm |
| Interoperability | Mandates interoperability between standardized coil assemblies | Analyzed interoperability with non-polarized and polarized coils |

The structure of the remaining paper is as follows: Section 2 presents the IPT configuration, followed by the design and modeling of the LCC-S compensation network-based IPT system. Section 3 provides the design of the proposed SBP. Section 4 compares the proposed magnetic SBP coupler with existing bipolar pads based on simulated results. This is followed by a study of compatibility strength between the proposed magnetic coupler as Tx and rectangular NPP and bipolar PP as Rx. The remaining Section 5 provides an extensive verification of the proposed SBP performance through an experimental prototype, followed by a discussion of the simulation results. Section 6 gives the conclusion.

## 2. IPT System

A typical block diagram of an IPT system for EV powering is shown in Figure 1 [25]. Generally, real-time EV charging through an IPT technique faces more airgap distance between charging pads, resulting in more leakage flux and relatively lesser mutual inductance between transmitter and receiver pads ($M_{TR}$) with a poor coupling coefficient ($k$). The relation between $M_{TR}$, the leakage inductance, and $k$ is given as

$$M_{TR} = L_T - L_1 = L_R - L_2 \quad (1)$$

$$k = \frac{M_{TR}}{\sqrt{L_T\, L_R}} \quad (2)$$

where $L_T$ and $L_R$ are self-inductances, and $L_1$ and $L_2$ are the leakage inductances of the Tx and Rx pads. In addition, the compensation network minimizes the VA rating on the primary side and maximizes the output efficiency on the secondary side [26]. The conventional compensation topologies in which the capacitor and inductor are connected in different series-parallel combinations have been commonly incorporated into the IPT charging system [27]. Various hybrid topologies have been preferred for the betterment of tuning controllability to attain constant voltage (CV) and constant current (CC) output characteristics, irrespective of load variation [28,29]. The compensation topologies series-series (SS), LCC-series, and LCC-LCC are recommended for the WPT system, considering their capability of providing high efficiency, zero voltage switching (ZVS) operation, and better interoperable performance with various compensation networks [30].

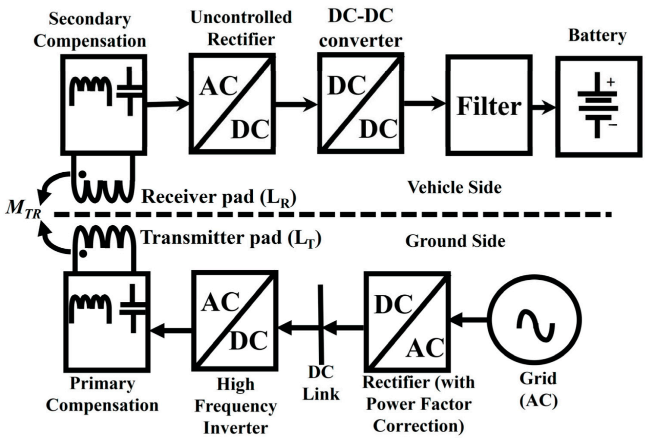


**Figure 1.** Block diagram of a complete IPT-based wireless EV charging system [25].

## 2.1. Modeling of LCC-S-Based IPT System

The generalized block diagram of a wireless charging system incorporating LCC-S-based compensation circuit is shown in Figure 2a, and its corresponding equivalent model is obtained by applying fundamental harmonic approximation (FHA) in Figure 2b.

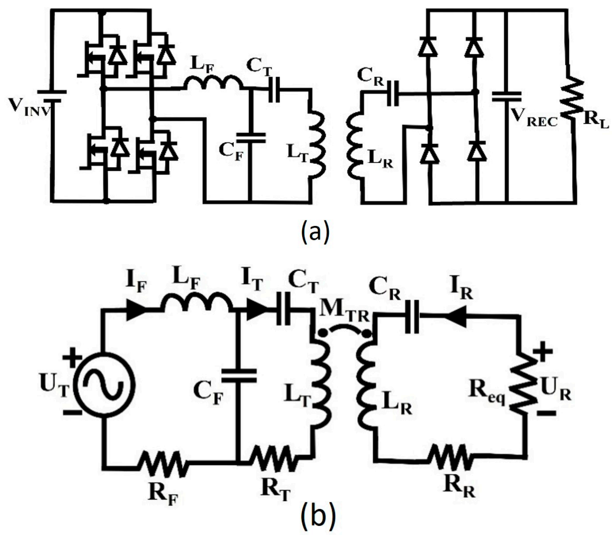


**Figure 2.** LCC-S-based IPT system: (**a**) circuit; (**b**) equivalent model.

In Figure 2a, $V_{INV}$ and $V_{REC}$ are the DC voltage of the primary side inverter and the secondary side rectifier. $L_F$, $C_F$, and $C_T$ are the compensating inductors and capacitors of the transmitter side, whereas $C_R$ is the compensating capacitor of the receiver side. $L_T$ and $L_R$ are the self-inductances of the Tx and Rx pads. The load resistance is denoted by $R_L$. In the equivalent circuit Figure 2b, $U_T$ and $U_R$ are the fundamental AC voltages of the primary side inverter and the secondary side rectifier. $I_F$, $I_T$, and $I_R$ are the corresponding currents flowing through the equivalent series resistance (ESR) $R_F$, $R_T$, and $R_R$. The mutual inductance between Tx and Rx coils is given by $M_{TR}$, and $R_{eq}$ is the equivalent load resistance.

The compensation network components are designed to maintain the circuitry resonance conditions at the operating frequency, such that $\omega_o = 2\pi f_o$ where $f_o$ is the operating frequency in Hertz. The design of the LCC-S compensation network is as follows: the compensation inductor and capacitors are derived from the angular resonance frequency, which can be expressed as

$$\omega_o = \frac{1}{\sqrt{L_F C_F}} = \frac{1}{\sqrt{L_R C_R}} = \frac{1}{\sqrt{(L_T - L_F)C_T}} \tag{3}$$

According to the FHA

$$U_T = \frac{2\sqrt{2}}{\pi} V_{INV},\ U_R = \frac{2\sqrt{2}}{\pi} V_{REC},\ R_{eq} = \frac{8}{\pi^2} R_L \tag{4}$$

Extracting mesh equations by applying Kirchhoff's Voltage Law (KVL) on equivalent models and neglecting ESR

$$U_T = (j\omega_o L_F + \frac{1}{j\omega_o C_F}) I_F - \frac{1}{j\omega_o C_F} I_T \tag{5}$$

$$(j\omega_o L_T + \frac{1}{j\omega_o C_F} + \frac{1}{j\omega_o C_T}) I_T - \frac{1}{j\omega_o C_F} I_F + j\omega_o M_{TR} I_R = 0 \tag{6}$$

$$(j\omega_o L_R + \frac{1}{j\omega_o C_R} + R_{eq}) I_R + j\omega_o M_{TR} I_T = 0 \tag{7}$$

using (3) in (5), (6) and (7) to obtain the current and voltage as below

$$I_T = \frac{U_T}{\omega_o L_F} \tag{8}$$

$$I_R = \frac{M_{TR}}{L_F} \frac{U_T}{R_{eq}} \tag{9}$$

$$I_F = (\frac{M_{TR}}{L_F})^2 \frac{U_T}{R_{eq}} \tag{10}$$

$$V_{REC} = \frac{M_{TR}}{L_F} V_{INV} = \frac{k\sqrt{L_T L_R}}{L_F} V_{INV} \tag{11}$$

The input VA rating is

$$VA_{in} = U_T I_F \tag{12}$$

and the input power factor ($PF_{in}$) is the phase angle difference between the inverter output voltage and current ($U_T$ and $I_F$), which can be expressed as

$$PF_{in} = \cos(\Theta_{in}) \tag{13}$$

The VA rating for the compensation element is

$$VA_{L_F} = {I_F}^2 \omega_o L_F,\ VA_{C_F} = \frac{{I_{C_F}}^2}{\omega_o C_F},\ VA_{C_T} = \frac{{I_T}^2}{\omega_o C_T},\ VA_{C_R} = \frac{{I_R}^2}{\omega_o C_R} \tag{14}$$

$$I_{C_F} = I_F - I_T \tag{15}$$

The output power and efficiency can be given as

$$P_O = (\frac{M_{TR}}{L_F})^2 \frac{V_{INV}}{R_L} \tag{16}$$

$$\eta = \frac{P_O}{P_O + I_F{}^2 R_F + I_T{}^2 R_T + I_R{}^2 R_R} \tag{17}$$

### *2.2. Theoretical Observation and Design Consideration*

It is noted from (11) that the output voltage is not dependent on load variation at constant $k$, which clearly implies that the LCC-S compensation network-based IPT system will maintain constant output voltage (CV) characteristics for EV charging. It is also understandable that the output voltage can be controlled by the charging pad parameters, including the self-inductance of Tx and Rx coils ($L_T$ and $L_R$), mutual inductance between charging pads ($M_{TR}$), and coupling coefficient ($k$). This clarifies that these parameters are essential for the designer involved in the design of a magnetic coupler structure for the wireless EV charging system.

Table 3 furnishes the design values for the parameters of the proposed IPT charging system. Equations (3) and (11) are used for the design of compensation elements $L_F$, $C_F$, $C_T$, and $C_R$ for the obtained self-inductance value of segmented BP, RP, and BP pads from the simulation using ANSYS Electronics Desktop 2025 R2. The minimum DC link capacitance value has been fixed using the following formula for the duty cycle (D = 0.5) and operating frequency ($f_o$ = 100 kHz).

$$C_{min} = \frac{I_{out} * \ D * \ (1 - D) * 1000}{f_O * \ V_{PP(max)}} \tag{18}$$

where the $I_{out}$ is the output current, and $V_{pp(max)}$ is the peak-to-peak ripple voltage.

**Table 3.** Parameters of the IPT system.

| Parameters | Segmented-BP | Non-Polarized (RP) | Polarized (BP) |
|---|---|---|---|
| $V_{INV}$ | 300 V | 300 V | 300 V |
| $f_o$ | 100 kHz | 100 kHz | 100 kHz |
| $R_L$ | 10Ω | 10Ω | 10Ω |
| $C_{min}$ | 300 µF | 300 µF | 300 µF |
| $L_F$ | 63.31 µH | 48.85 µH | 40.13 µH |
| $C_F$ | 40 nF | 51.84 nF | 63.11 nF |
| $C_T$ | 14.61 nF | 16.99 nF | 16.98 nF |
| $C_R$ | 10.83 nF | 12.90 nF | 13.41 nF |

## 3. Design of Magnetic Coupler

The structure of the proposed and existing magnetic coupler is depicted in Figure 3. The total number of turns in the conventional BP has been split and forms the separated layers as a segmented (S) coil known as a segmented bipolar pad (SBP). The notable characteristics of the segmented coil are its polarized nature, which allows uniform magnetic flux distribution across the pad area. Consequently, the parallel flux path effectively improves the flux linkage between the transmitter and receiver pads. The significance of the segmented coil lies in the improved tolerance to misalignment and better compatibility with other coil configurations. Figure 3a shows a clear view of a single-segmented BP (SSBP) coil in which the S coil ($Tx_3$) dimension has been chosen to maximize the coupling strength between the Tx and Rx pad to give better misalignment tolerance. The radius of the inner S coils has been decreased as the number of segmentations increases, producing double-segmented BP (DSBP) as presented in Figure 3b.

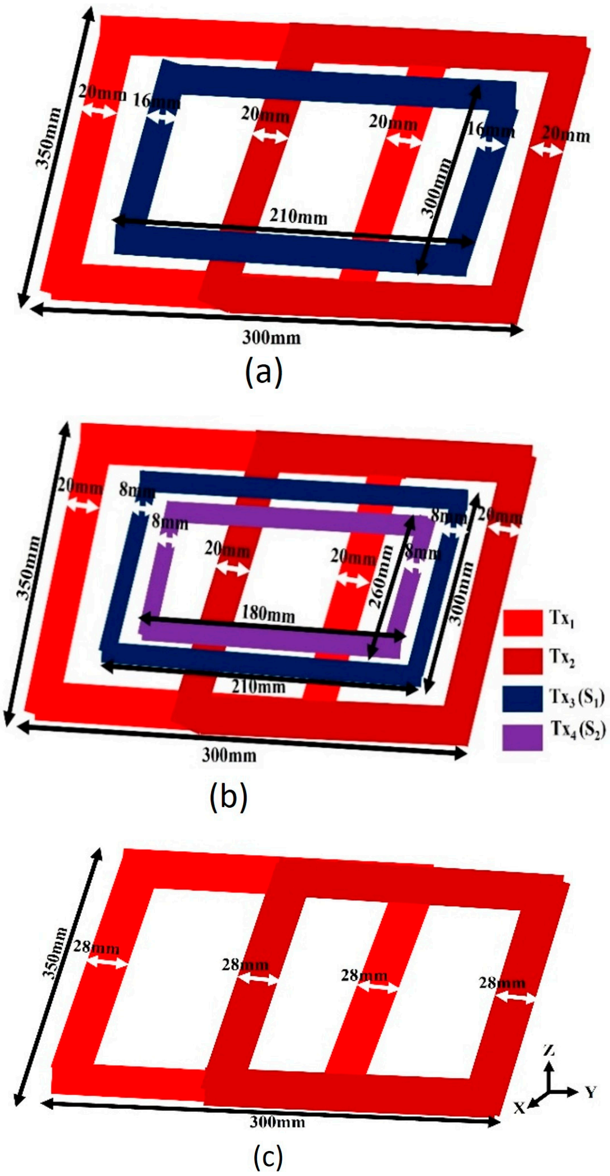


**Figure 3.** Structure of magnetic coupler: (**a**) proposed single-segmented BP (SSBP); (**b**) proposed double-segmented BP (DSBP); (**c**) existing BP.

The proposed segmented BP charging pad has been developed to attain improved misalignment tolerance strength and better interoperability performance based on the finite-element-based design refinement process, as shown in Figure 4. The paper considers the design of single- and double-segmented BP coils to analyze the performance of the proposed magnetic coupler. The number of segmentations in the proposed pad can be fixed as per the requirement of a better misalignment tolerance rate and enhanced interoperability characteristics in real-time applications. It needs to be mentioned that the design parameters, including outer dimensions, inner air gap, number of turns, turn thickness, and distance between each turn, are set to be identical for the proposed and existing magnetic couplers to conduct a genuine comparison. For simplicity, the Rx pad has been designed identically to its corresponding Tx pad for analyzing the performance of the proposed pad against lateral misalignment. In the case of interoperability evaluation, the Tx pad of the proposed and conventional magnetic coupler is simulated with a non-polarized and polarized Rx pad. Table 4 provides the design parameters, which imply that identical geometrical dimensions have been utilized to design the proposed and existing charging pads.

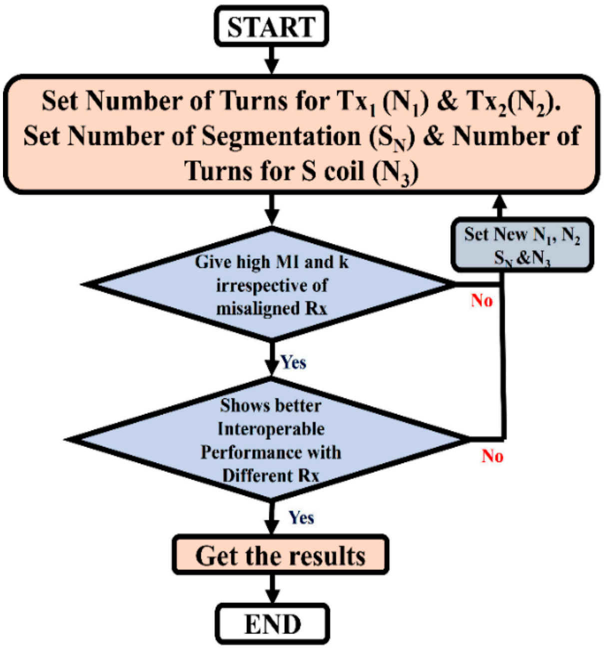


**Figure 4.** Flowchart for the design process of segmented BP.

**Table 4.** Design parameters for charging pads.

| Types | Structure | Parameters | |
|---|---|---|---|
| BP |  | Outer dimensions of pad | 300 mm × 350 mm |
| SSBP |  | Total number of turns | 28 |
| DSBP | 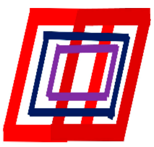 | Each turn thickness | 2 mm |

## 4. Performance Evaluation

The performance of the proposed SBP charging pad is investigated based on the functionality comparison with existing BP pads. According to the finite-element-based design refinement process, the single-segmented and double-segmented bipolar pads (SSBP and DSBP) have been designed using ANSYS Maxwell software. The magnetic flux density (*B*) and magnetic field strength (*H*) of the proposed SSBP, DSBP, and existing BP magnetic couplers are shown in Figure 5. The distribution of flux components shown in Figure 5 is simulated at a 100 mm vertical distance between the Tx and Rx pads. Figure 5a,b shows the *B* field of the proposed SSBP and existing BP in the isometric views. It has been noted that a higher *B* field is attained in the proposed SSBP than in the existing BP pad. It has been observed from Figure 5a that the magnetic flux of the SSBP is distributed uniformly across the entire pad region compared to the BP in Figure 5b. This ensures that the effective flux path is obtained in the proposed pad. Figure 5c,d gives the *H* field of SSBP and BP at the perfectly aligned condition; whereas, Figure 5e shows the laterally misaligned SSBP with the *H* value. The maximum *H* field obtained for the laterally misaligned SSBP is shown in Figure 5e, which is higher than the *H* field of the perfectly aligned BP in Figure 5d. This confirms the better performance of the proposed SSBP against lateral misalignment. Figure 5f gives the isometric view of the DSBP with magnetic flux density.

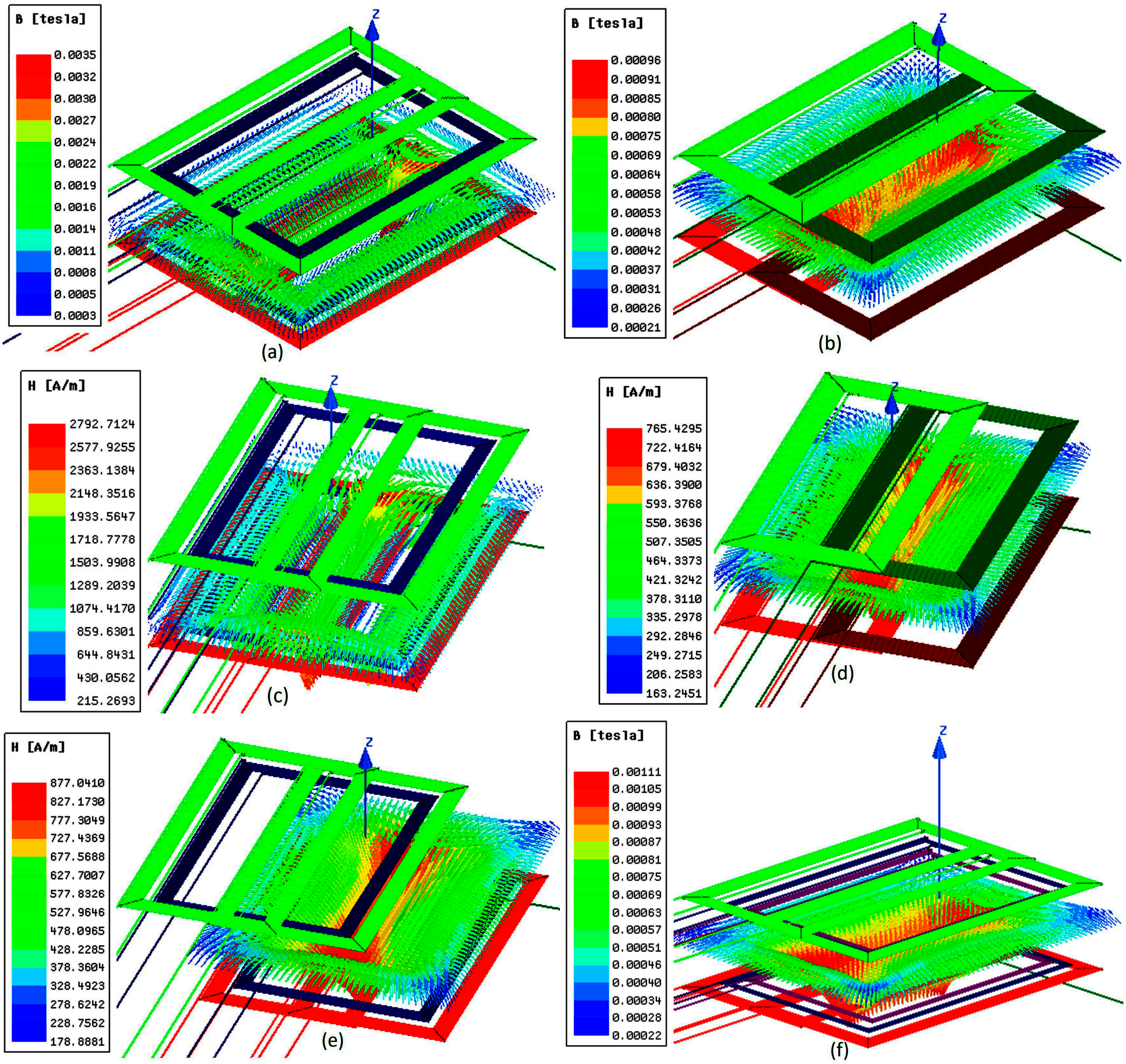


**Figure 5.** Flux distribution at 100 mm vertical air gap between Tx and Rx pads: (**a**) SSBP with *B* field; (**b**) BP with *B* field; (**c**) SSBP with *H* field; (**d**) BP with *H* field; (**e**) misaligned SSBP with *H* field; (**f**) DSBP with *B* field.

*Magnetic Field Characteristics*

The magnetic field characteristics in terms of magnetic flux density (*B*) and magnetic field strength (*H*) for the proposed and conventional pads are given in Figure 5. For the detailed analysis, the distribution of the magnetic flux and the intensity of the magnetizing field over the charging pad region for the SSBP and BP are shown in Figure 6a,b. It is noted from Figures 5c,d and 6b that the proposed SSBP exhibits a magnetizing field maximum of 2792 A/m, which is considerably higher than the BP with a magnitude of 765 A/m. Consequently, the maximum amount of *B* distribution created by the SSBP pad is 0.0035 T, which is higher than the maximum *B* value of 0.00096 T of the BP pad, as shown in Figures 5a,b and 6a. The obtained *H* and *B* values of SSBP are 3.65 times higher than the magnetic field characteristics of BP. This improvement is attained because of the polarized nature of the segmented coil in the proposed SSBP. The appropriate geometrical structure and proper turn distribution of SSBP will significantly enhance the magnetic field strength, leading to enhanced flux concentration in the proposed pad. Moreover, uniformity in the distribution of the magnetic flux throughout the entire pad region offers better flux linkage between the transmitter and the receiver pads of SSBP when compared to BP. The enhanced magnetic characteristics directly contribute to improved coupling coefficient and mutual inductance of SSBP. Subsequently, SSBP facilitates better power transmission compared to the BP. Meanwhile, analyzing the performance of the proposed pad in the misaligned condition based on the magnetic field characteristics from Figure 5e, the magnitude of *H* for SSBP is 877 A/m; whereas, the value of *H* for perfectly aligned BP is 765 A/m, as shown in Figure 5d, which is less than the magnetic field strength of SSBP at the misaligned condition. Thereby, it has been established that the proposed pad exhibits superior performance even in the misaligned scenarios compared to aligned BP. The improved magnetic characteristics of the proposed pad validate the significance of SSBP over conventional BP.

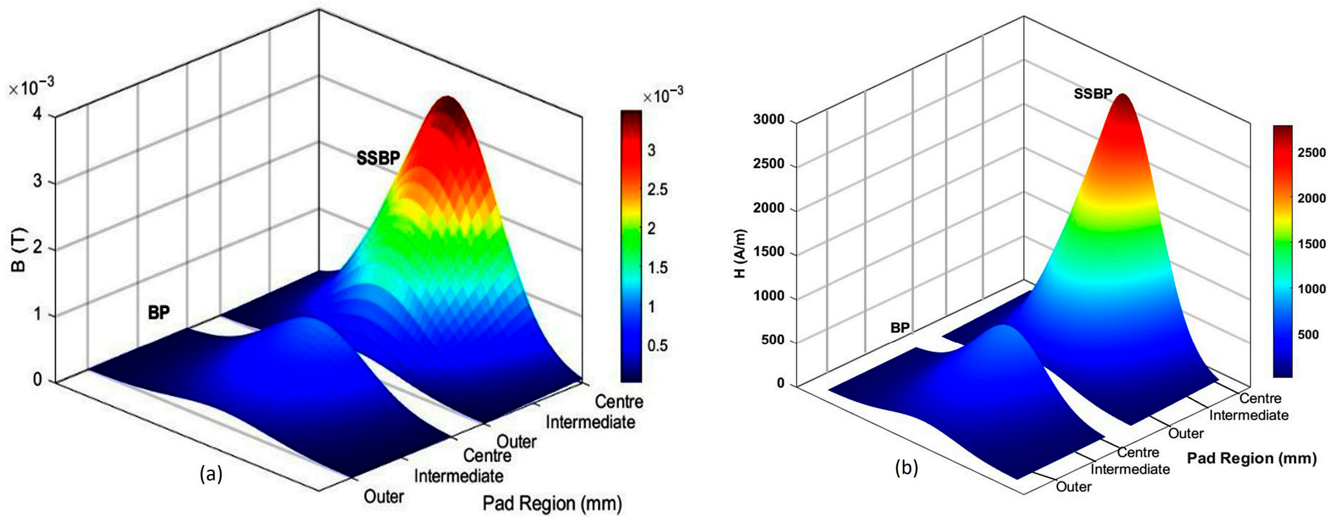


**Figure 6.** Magnetic field comparison between the proposed and conventional pad: (**a**) magnetic flux density; (**b**) magnetic field strength.

It has been observed from Figure 6 that a high amount of magnetic field passes through the center region of the pad. The moderate distribution of *B* and *H* was obtained in the intermediate region, and the lower concentration in the outer region of the pad. The amount of magnetic flux and magnetic field strength is high at the center of the pad, and gradually the concentration of *B* and *H* reduces towards the outer pad area.

Based on the finite element analysis (FEA), the interoperability performance between each and every transmitter and receiver coil for the three types of charging pads is presented in Table 5. Table 5 provides the cross-coupling effect between each of the transmitter and receiver coils in terms of mutual inductance and the coupling coefficient. For the SSBP, it can be observed that the cross-coupling for $Tx_1$-$Rx_1$, $Tx_2$-$Rx_2$, and $Tx_3$-$Rx_3$ is large, and the cross-coupling for $Tx_1$-$Rx_2$ and $Tx_2$-$Rx_1$ is reduced. Similarly, the cross-coupling effect for the BP and DSBP can be analyzed based on the values given in Table 5.

**Table 5.** Mutual inductance and coupling coefficient between each transmitter and receiver coils.

| Charging Pads | Coil Combinations | Mutual Inductance (μH) | Coupling Coefficient |
|---|---|---|---|
| BP | $Tx_1$ and $Rx_1$ | 10.85 | 0.1253 |
| | $Tx_1$ and $Rx_2$ | 3.61 | 0.042 |
| | $Tx_2$ and $Rx_1$ | 3.56 | 0.041 |
| | $Tx_2$ and $Rx_2$ | 10.94 | 0.129 |
| SSBP | $Tx_1$ and $Rx_1$ | 6.79 | 0.118 |
| | $Tx_1$ and $Rx_2$ | 2.37 | 0.041 |
| | $Tx_1$ and $Rx_3$ | 5.13 | 0.1053 |
| | $Tx_2$ and $Rx_1$ | 2.38 | 0.041 |
| | $Tx_2$ and $Rx_2$ | 6.94 | 0.122 |
| | $Tx_2$ and $Rx_3$ | 5.31 | 0.109 |
| | $Tx_3$ and $Rx_1$ | 5.1 | 0.1049 |
| | $Tx_3$ and $Rx_2$ | 5.26 | 0.1091 |
| | $Tx_3$ and $Rx_3$ | 6.26 | 0.1517 |
| DSBP | $Tx_1$ and $Rx_1$ | 6.8 | 0.1184 |
| | $Tx_1$ and $Rx_2$ | 2.36 | 0.0417 |
| | $Tx_1$ and $Rx_3$ | 2.59 | 0.093 |
| | $Tx_1$ and $Rx_4$ | 2.13 | 0.083 |
| | $Tx_2$ and $Rx_1$ | 2.38 | 0.0415 |
| | $Tx_2$ and $Rx_2$ | 6.93 | 0.122 |
| | $Tx_2$ and $Rx_3$ | 2.82 | 0.1022 |
| | $Tx_2$ and $Rx_4$ | 2.63 | 0.1027 |
| | $Tx_3$ and $Rx_1$ | 2.58 | 0.094 |
| | $Tx_3$ and $Rx_2$ | 2.78 | 0.1026 |
| | $Tx_3$ and $Rx_3$ | 1.66 | 0.1261 |
| | $Tx_3$ and $Rx_4$ | 1.5 | 0.1229 |
| | $Tx_4$ and $Rx_1$ | 2.11 | 0.0835 |
| | $Tx_4$ and $Rx_2$ | 2.58 | 0.1033 |
| | $Tx_4$ and $Rx_3$ | 1.5 | 0.1232 |
| | $Tx_4$ and $Rx_4$ | 1.44 | 0.1276 |

The total mutual inductance ($M_{TR}$) between the transmitter (Tx) and receiver (Rx) pads is the summation of the absolute values of the mutual inductance between each coil of the transmitter and receiver, which can be calculated by Equation (19).

$$M_{TR} = \sum_{i=1}^{n} \sum_{j=1}^{n'} M_{TX_i RX_j} \quad (19)$$

Similarly, the self-inductance of the Tx pad $L_T$ and Rx pad $L_R$ is the sum of the self-inductance of each coil of the transmitter and receiver. Thereby, the coupling coefficient can be obtained from Equation (20).

$$k = \frac{M_{TR}}{\sqrt{(\sum_{i=1}^{n} L_{TX_i})(\sum_{i=1}^{n'} L_{RX_j})}} \quad (20)$$

where $n$ is the number of coils in the transmitter pad and $n'$ is the number of coils in the receiver pad.

The simulation results of mutual inductance between transmitter and receiver pads ($M_{TR}$) and coupling coefficient ($k$) for the proposed and existing charging pads under lateral misalignment (ΔY) from −90 mm to +90 mm against a 100 mm vertical distance between Tx and Rx pads are shown in Figure 7. The graphical plots are depicted in Figure 7 for different designs of magnetic couplers, where the Rx pad is identical to its corresponding Tx pad for simplicity.

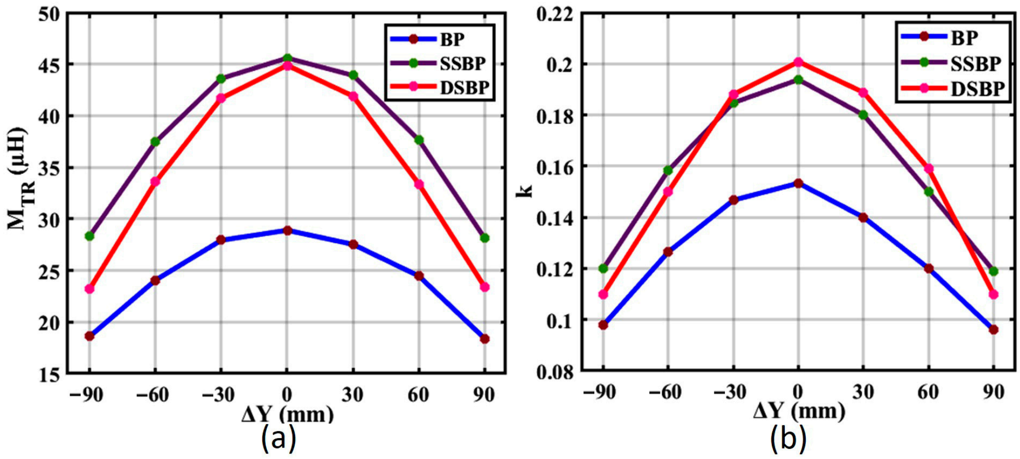


**Figure 7.** Lateral misalignment for proposed and existing magnetic couplers: (**a**) $M_{TR}$; (**b**) $k$.

From Figure 7, it is observed that the different designs of magnetic couplers have shown a drastic influence on both the flux distribution and the strength of coupling between the Tx and Rx pads. It is also noted that the impact of the lateral misalignment is reflected in the variation in $M_{TR}$ and $k$. Similar results are obtained for both left and right side ΔY, since an identical misalignment distance has been considered in the paper. It is noted from the simulated results that the $M_{TR}$ and $k$ values have been inevitably higher for the proposed SBP than the existing BP magnetic couplers. For the perfectly aligned condition, the proposed magnetic coupler design shows 57% improvement in $M_{TR}$ with a significant coupling coefficient value of $k$ = 0.19 for the SSBP and $k$ = 0.2 for the DSBP when compared with the existing BP. Similarly, at ΔY = ±90 mm, the SSBP shows 52%, and the DSBP shows 24% higher $M_{TR}$ value with better $k$ than the BP pad. Meanwhile, the simulation results imply that the ±90 mm laterally misaligned SSBP transfer equal $M_{TR}$ of a properly aligned BP. Thereby, the high misalignment tolerance capability of the proposed SBP has been undoubtedly noticed from the simulated results.

The LCC-series connected IPT system has been simulated using MATLAB R2023b software, and the variation in output power and DC-DC efficiency for the proposed and existing charging pads is studied. The graphical plots depicted in Figure 8 provide the relationship between the output power ($P_O$) and DC-DC efficiency ($\eta$) versus lateral misalignment for 100 mm vertical separation. It has been observed from Figure 8a that the output power gradually decreases when the ΔY distance increases for any type of charging pad. The LCC-series compensation circuit shows that output power and DC-DC efficiency are almost stable by facilitating a constant voltage (CV) output irrespective of the misaligned conditions. The proposed charging pads attain a maximum power output ($P_{Omax}$) of 4.7 kW, comparatively. The $P_O$ of the SSBP and DSBP at ΔY = 0 is 5.5% more than the BP at aligned conditions.

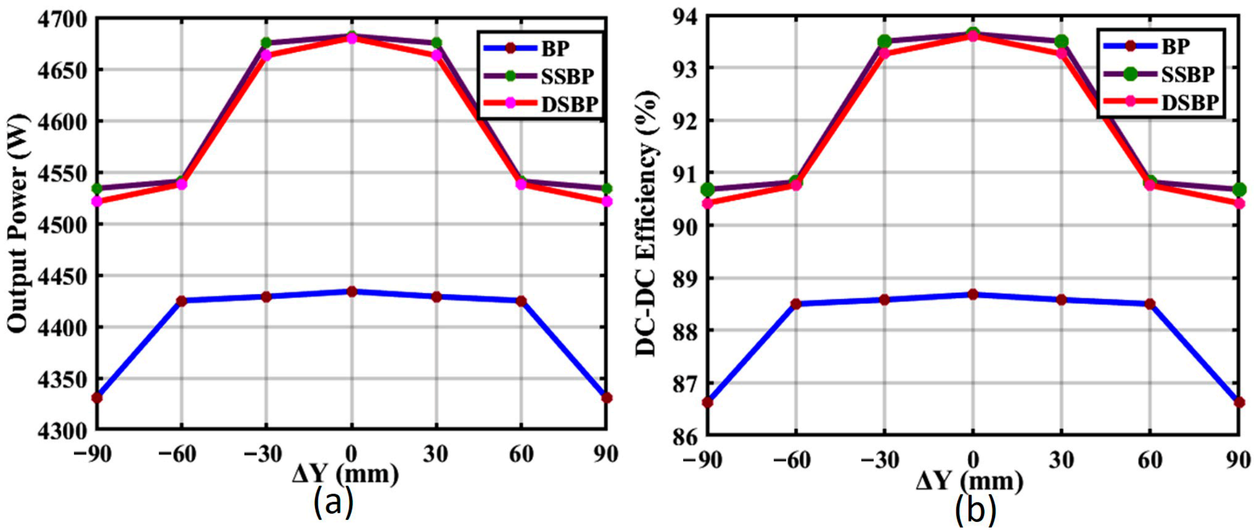


**Figure 8.** Lateral misalignment for proposed and existing magnetic couplers: (**a**) output power; (**b**) DC-DC efficiency.

Meanwhile, analyzing the simulated results of the horizontally misaligned SBP, the $P_O$ of the proposed SBP at ΔY = ±90 mm is 2.2% more than the $P_O$ of the perfectly aligned existing BP. It is clear from the investigation that the SSBP and DSBP have better tolerable capability for a wide range of lateral misalignment. Similarly, the SBP shows a maximum efficiency of 93.64%, which is 4.96% greater than the highest efficiency attained by the existing BP. The modest rise in coupling coefficient for the proposed pad leads to enhanced power transmission and overall efficiency, which implies the system is operating under a resonant condition. Thereby, the systematic design refinement process has been effectively utilized to design a magnetic coupler with a better misalignment tolerance rate.

To study the interoperability nature of the proposed pad, the Tx coil has been set as the existing BP and the newly designed single-segmented BP; whereas, the Rx coil has been chosen as a non-polarized RP and polarized BP pads. The graphical plots are depicted in Figure 9, representing the mutual inductance and coupling coefficient between transmitter and receiver pads against the lateral axis misalignment at 100 mm separation at the Z-axis. The plot showing the interoperable performance of four cases includes BP-RP, SSBP-RP, BP-BP, and SSBP-BP. As noted, the interoperable performance of SSBP as a Tx pad with both unipolar (RP) and bipolar (BP) Rx pads is comparatively higher than the existing BP coupler working with different Rx pads. At the perfectly aligned condition, the performance of the SSBP as a Tx pad with the non-polarized RP pad shows 24% higher $M_{TR}$ with a relatively larger coupling coefficient than the BP (Tx pad) functioning with the RP (Rx pad) for the aligned condition. Similarly, the proposed pad with polarized BP gives 25% more $M_{TR}$ compared with BP-BP performance. The effective interoperable characteristics of the proposed SBP magnetic coupler have been confirmed from the simulated results of mutual inductance ($M_{TR}$) and coupling coefficient ($k$).

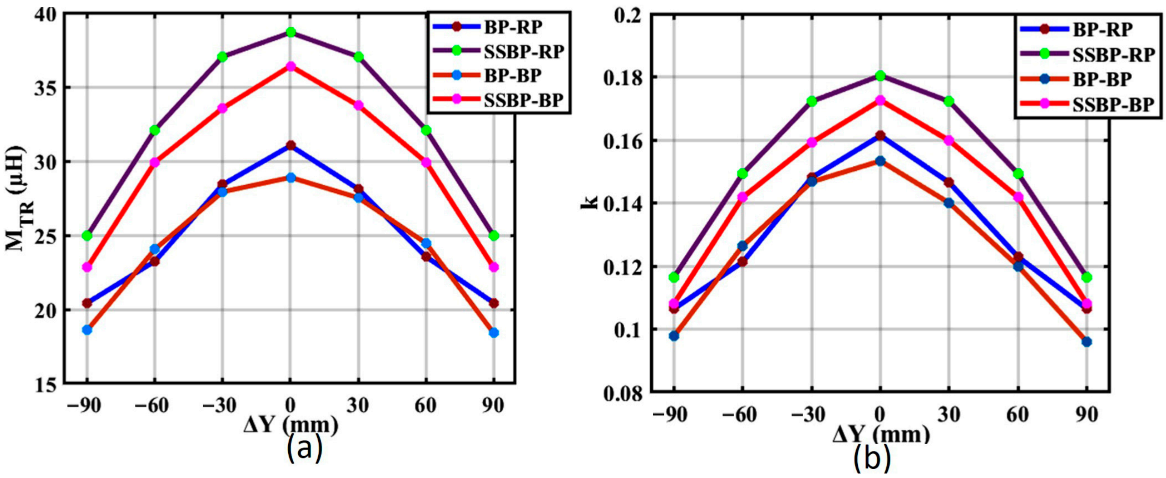


**Figure 9.** Interoperability performance of proposed and existing magnetic couplers: (**a**) $M_{TR}$; (**b**) $k$.

For the BP and SSBP, the simulated $P_O$ and $\eta$ for the interoperability performance varying with lateral misalignment have been shown in Figure 10. Compared with the interoperable nature of existing BP pads, higher power output and system efficiency have been attained for the proposed SSBP as a Tx pad with both non-polarized and polarized Rx pads. The maximum $\eta$ improvement is 2.46%, and 3.7% is obtained for SSBP with non-polarized and polarized pads compared to the interoperable performance of BP with non-polarized and polarized pads.

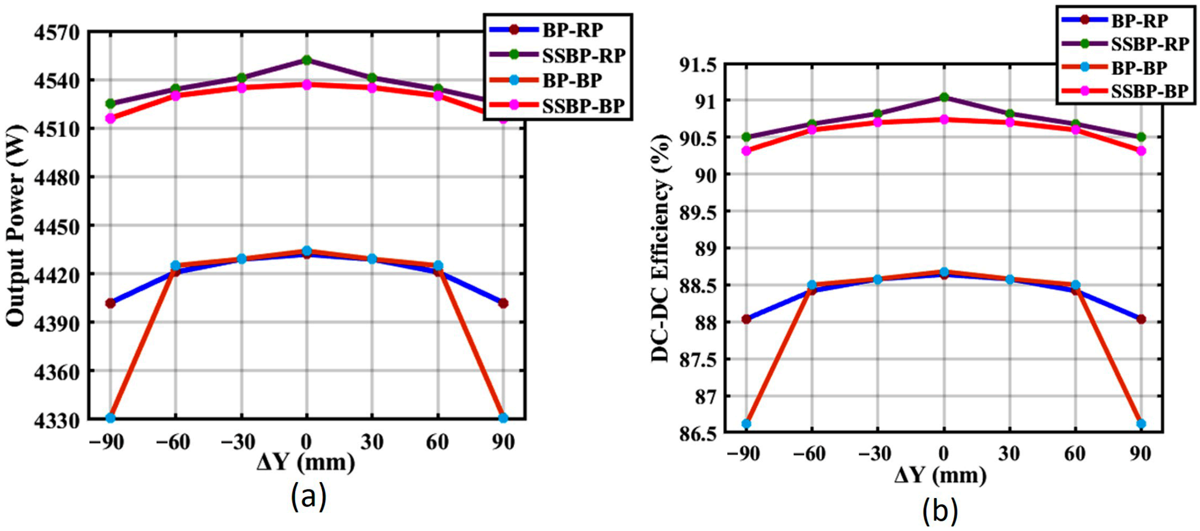


**Figure 10.** Interoperability performance of proposed and existing magnetic couplers: (**a**) output power; (**b**) DC-DC efficiency.

## 5. Experimental Verification

A prototype system has been constructed to validate the performance of the proposed SBP pad. Based on the simulation results, the SSBP and DSBP show better performance than existing BP, which ensures the SSBP gives the maximum power transmission characteristics. Thereby, the comparative study has been carried out for the proposed SSBP and existing BP through a laboratory setup. The experimental parameters of the IPT hardware system are listed in Table 6, whereas Table 7 provides the specifications for the hardware equipment utilized in this paper.

**Table 6.** Parameters of the prototype system.

| Parameters | | Values |
|---|---|---|
| $V_{dc}$ | | 31 V |
| $f_o$ | | 100 kHz |
| $V_{Omax}$ | | 25.7 V |
| $I_{Omax}$ | | 8.42 A |
| $P_{Omax}$ | | 216 W |
| Compensation elements values | SSBP | $L_F$ = 50 µH<br>$C_F$ = 57 nF<br>$C_T$ = 15 nF<br>$C_R$ = 12 nF |
| | BP | $L_F$ = 27 µH<br>$C_F$ = 91 nF<br>$C_T$ = 19 nF<br>$C_R$ = 15 nF |

**Table 7.** Specifications of the hardware components.

| Equipment | Part No. | Rating |
|---|---|---|
| SiC MOSFET (Littlefuse, Chicago, IL, USA) | LSIC1MO120E0080 | 1200 V, 25 A |
| FPGA Controller (Intel Corporation (formerly Altera), Santa Clara, CA, USA) | EP4CE30F23C7N | - |
| Diode (onsemi, Scottsdale, AZ, USA) | FFPF10U20DP | 200 V, 10 A |
| DSO (Keysight Technologies, Santa Rosa, CA, USA) | EDUX1002G | Up to 50 MHz |
| LCR meter (Hioki E.E. Corporation, Nagano, Japan) | IM 3536 | Up to 8 MHz |
| Clamp Meter (Center Technology Corp., New Taipei City, Taiwan, China) | CENTER 222_ AC/DC | Up to 600 V, 600 A |

The IPT system shown in Figure 11a consists of a DC power source, a high-frequency inverter (HFI) operating at $f_o$ = 100 kHz, an LCC-S compensation circuit, SSBP magnetic couplers, an uncontrolled rectifier, a filter capacitor, and a resistive load. Figure 11b provides the fabrication photo of the proposed structure. The voltage across the SSBP transmitter pad and receiver pad with the compensation circuit has been measured as 29.2 V and 27.5 V is shown in Figure 11c. The maximum load voltage ($V_{Omax}$) is 25.7 V for the given 31 V input voltage ($V_{dc}$) from the DC power source, and the maximum load current ($I_{Omax}$) is 8.42 A, as shown in Figure 11d. The obtained maximum output power ($P_{Omax}$) is 216 W with a DC-DC efficiency of 88%.

To validate the working of the proposed pad through experimental results, the $P_O$ and $\eta$ have been measured for the existing BP and SSBP for the lateral misalignment condition $\Delta$Y = −90 mm to 0 mm against a 100 mm vertical distance, as shown in Figure 12. From Figure 12a, the existing BP measured the maximum output power of 205.4 W with 81% DC-DC efficiency for the perfectly aligned case. Whereas for horizontally misaligned conditions, the $P_O$ and $\eta$ of the BP drop and show 198 W with 73% at $\Delta$Y = −90 mm. Looking into the results of SSBP performance from Figure 12b, the proposed pad shows a maximum output power of 216 W for perfectly aligned conditions and a minimum output power of 207.5 W at $\Delta$Y = −90 mm lateral misalignment case. Similarly, the DC-DC efficiency for SSBP, the pad measured a maximum of 88% and a minimum of 82% with respect to lateral misalignment. Based on the comparative analysis, it is observed from the measured values $P_O$ and $\eta$, that the performance of SSBP at $\Delta$Y = −90 mm is almost symmetrical to that of a perfectly aligned BP. The results reflect the better misalignment tolerance ability of the proposed SSBP pad over the existing BP. Meanwhile, the proposed SSBP measured 7% to 9% improved $\eta$ when compared with the existing BP. Minor discrepancies between the simulated and the experimental DC-DC efficiency are due to the hand-wound charging coils utilized for hardware. Despite these differences, the proposed novel SSBP has outperformed the existing BP, as evidenced by both the simulation and experimental results.

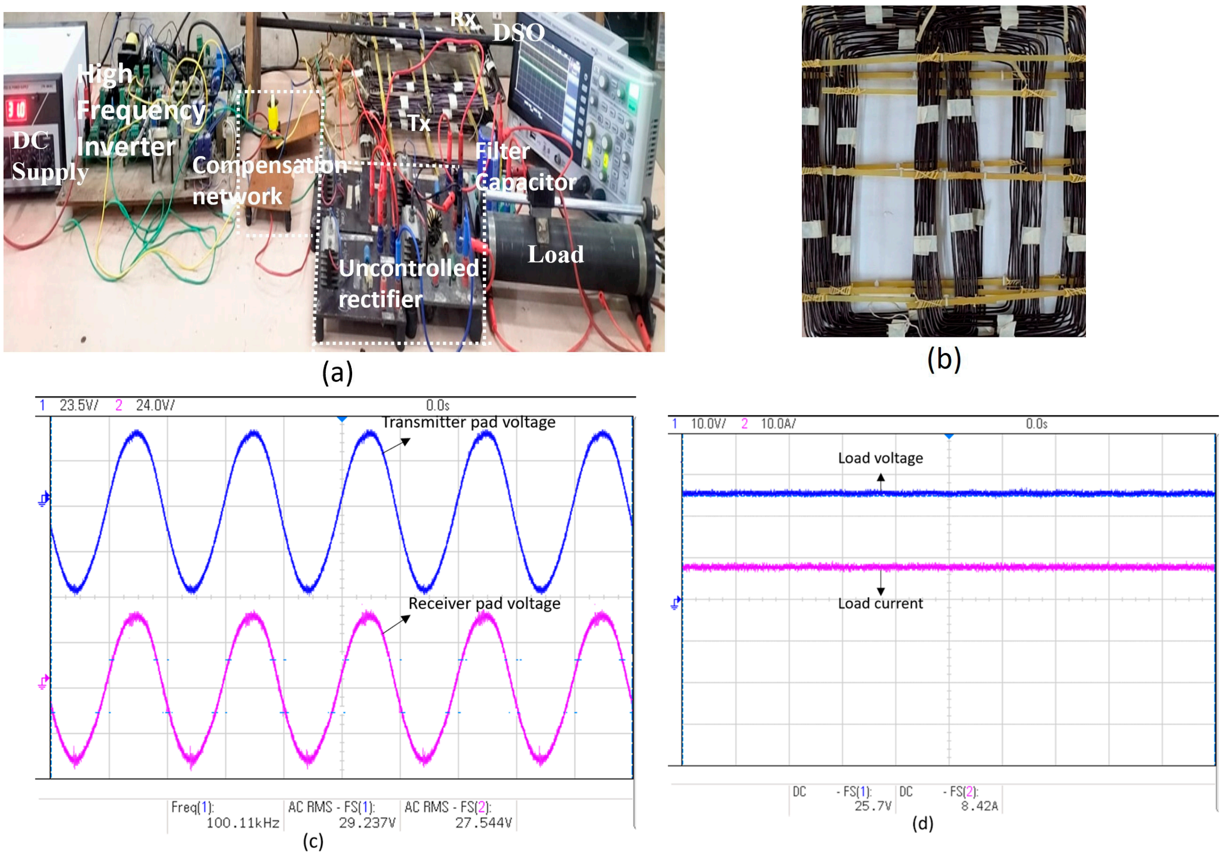


**Figure 11.** Experimental photo for SSBP: (**a**) IPT charging system with proposed SSBP; (**b**) SSBP fabrication image; (**c**) voltage across Tx and Rx pad; (**d**) load voltage and load current.

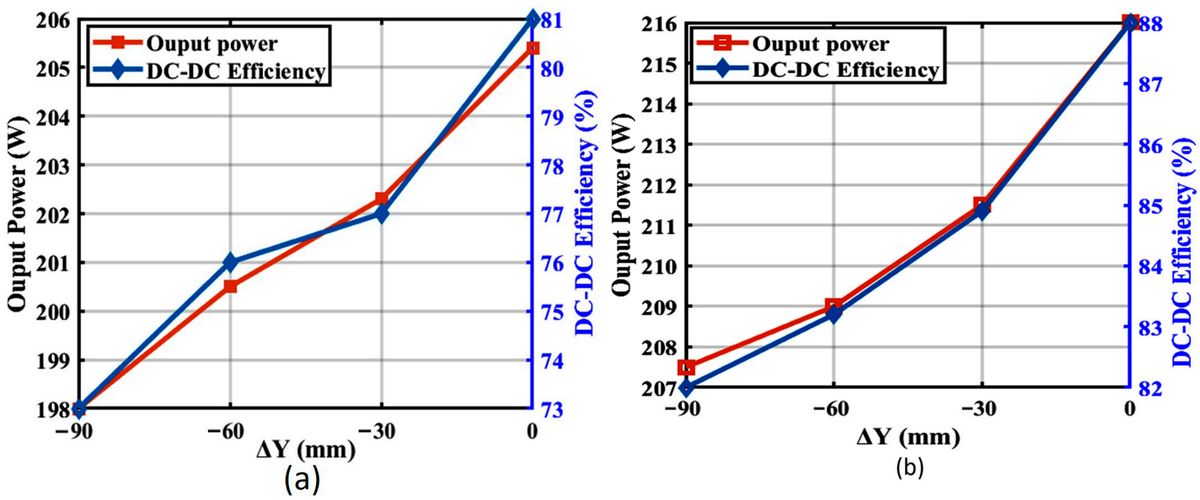


**Figure 12.** Experimental results: (**a**) existing BP; (**b**) proposed SSBP.

*Discussion*

Based on the simulation results, the proposed SBP magnetic coupler facilitates the following effective benefits when compared to the existing BP.

1. The maximum $M_{TR}$ of the proposed pad shows 57% enhancement with relatively larger $k = 0.19$ for SSBP and $k = 0.2$ for the DSBP at laterally aligned conditions.
2. The SSBP and DSBP show improved $M_{TR}$ values of 52% and 24% at $\Delta Y = \pm 90$ mm compared to BP.
3. The proposed SSBP and DSBP at $\Delta Y = 0$ mm give 5.5% more $P_o$ with an $\eta$ improvement of 4.96% compared to BP.
4. The $M_{TR}$ of SSBP at $\Delta Y = \pm 90$ mm is equal to the $M_{TR}$ values of BP at $\Delta Y = 0$ mm, which ensures the better misalignment tolerance characteristics of the proposed SSBP as implied in Figure 7a.
5. The interoperability performance of the proposed SSBP magnetic coupler with a non-polarized rectangular pad (RP) shows 24% improved $M_{TR}$ with $k = 0.18$ at $\Delta Y = 0$ mm and 22% higher $M_{TR}$ with $k = 0.12$ at $\Delta Y = \pm 90$ mm than BP-RP characteristics.
6. In the case of compatibility with the polarized pad, the SSBP-BP gives a maximum of 25% and a minimum of 20% better $M_{TR}$ value with improved $k$ compared to BP-BP performance.
7. The $P_o$ of SSBP-BP is relatively high with an improved $\eta$ of 3.7% over the values obtained for BP-BP magnetic coupler.

## 6. Conclusions

In this paper, a design modification was performed in the existing bipolar pad (BP) to propose a novel segmented bipolar pad (SBP) with symmetrical dimension parameters. The proposed SBP outperforms the conventional BP magnetic coupler in terms of improved mutual inductance between the transmitter and receiver pad ($M_{TR}$) and coupling coefficients ($k$). In the development of magnetic couplers as single-segmented bipolar pad (SSBP) and double-segmented bipolar pad (DSBP), a finite-element-based design refinement was adopted in the process of splitting up the number of turns into separate layers to form a segmented (S) coil. The polarized characteristics of the segmented coil exhibit uniform flux distribution between the transmitter and receiver pads. Owing to this effective flux path, the proposed pad attains improved misalignment tolerance and better interoperability. This work utilizes the inductor–capacitor–capacitor-series (LCC-S) compensation network to attain constant voltage (CV) output characteristics. A 4.7 kW IPT charging system incorporating LCC-S compensation topology with the proposed pad was simulated using MATLAB software to extract the output power ($P_o$) and DC-DC efficiency ($\eta$). The work presented in this paper extensively compares the proposed SBP with the existing BP based on the simulation output results. The comparison was made based on the following conditions: (1) lateral misalignment ($\Delta Y$) from $-90$ mm to +90 mm at 100 mm vertical separation, and (2) interoperability characteristics with non-polarized pad (NPP) and polarized pad (PP). The proposed SSBP shows 4.96% improvement in DC-DC efficiency under perfectly aligned conditions and about 4.06% $\eta$ rise at $\Delta Y = 90$ mm misalignment compared to the BP. For the interoperable performance of SSBP, the maximum $\eta$ improvement is 2.46% for non-polarized and 3.7% for polarized pads compared to the interoperability of BP. The proposed work has been experimentally verified by a laboratory prototype system as well. The experimental results show that the performance of the proposed pad is better than that of the conventional pad. It has been concluded that the proposed SBP magnetic coupler gives better misalignment tolerance and interoperable characteristics compared to the existing BP pad. This work is limited to static wireless EV charging, and the applicability of the proposed pad to dynamic charging remains for future studies. Since the proposed

https://doi.org/10.3390/en19051258

wireless charging system is rated at 4.7 kW for light-duty EVs, with smaller dimensions, it can be adopted in home and office parking areas. The proposed charging pad dimensions can be adjusted based on the application and its power rating.

**Author Contributions:** Conceptualization: B.M. and P.K.; writing—original draft preparation: B.M.; supervision: P.K. and B.R.; formal analysis: M.A.N. and M.S.; validation: B.R. and N.P.; funding acquisition: M.A.N., N.P. and P.K.; and writing—review and editing: P.K. and M.S. All authors have read and agreed to the published version of the manuscript.

**Funding:** This research received no external funding.

**Data Availability Statement:** All data generated or analyzed during this study are included in this published article.

**Conflicts of Interest:** The authors have no relevant conflicts of interest to disclose.

## References

1. Rabih, M.; Takruri, M.; Al-Hattab, M.; Alnuaimi, A.A.; Bin Thaleth, M.R. Wireless Charging for Electric Vehicles: A Survey and Comprehensive Guide. *World Electr. Veh. J.* **2024**, *15*, 118. [CrossRef]
2. Niu, S.; Jia, Q.; Hu, Y.; Yang, C.; Jian, L. Safety Management Technologies for Wireless Electric Vehicle Charging Systems: A Review. *Electronics* **2025**, *14*, 2380. [CrossRef]
3. Nebrida, A.P. Characterization of Resonant Coupled Inductor in a Wireless Power Transfer System. *J. Electr. Syst. Inf. Technol.* **2024**, *11*, 8. [CrossRef]
4. Chakibanda, V.; Komanapalli, V.L.N. Optimization in Magnetic Coupler Design for Inductively Coupled Wireless Charging of Electric Vehicle: A Review. *Arab. J. Sci. Eng.* **2023**, *48*, 14257–14294. [CrossRef]
5. Vishnuram, P.; Panchanathan, S.; Rajamanickam, N.; Krishnasamy, V.; Bajaj, M.; Piecha, M.; Blazek, V.; Prokop, L. Review of Wireless Charging System: Magnetic Materials, Coil Configurations, Challenges, and Future Perspectives. *Energies* **2023**, *16*, 4020. [CrossRef]
6. Xu, H.; Tan, L.; Gui, L.; Wu, Z.; Li, H.; Huang, X. Design of Magnetic Coupler for Wireless Power Transmission System Based on Magnetic Field Reconstruction. *IEEE Trans. Power Electron.* **2024**, *39*, 2855–2866. [CrossRef]
7. Song, K.; Lan, Y.; Zhang, X.; Jiang, J.; Sun, C.; Yang, G.; Yang, F.; Lan, H. A Review on Interoperability of Wireless Charging Systems for Electric Vehicles. *Energies* **2023**, *16*, 1653. [CrossRef]
8. Mohamed, A.A.S.; Shaier, A.A.; Metwally, H.; Selem, S.I. Interoperability of the Universal WPT3 Transmitter with Different Receivers for Electric Vehicle Inductive Charger. *eTransportation* **2020**, *6*, 100084. [CrossRef]
9. Luo, Z.; Wei, X. Analysis of Square and Circular Planar Spiral Coils in Wireless Power Transfer System for Electric Vehicles. *IEEE Trans. Ind. Electron.* **2018**, *65*, 331–341. [CrossRef]
10. Bandyopadhyay, S.; Venugopal, P.; Dong, J.; Bauer, P. Comparison of Magnetic Couplers for Ipt-Based Ev Charging Using Multi-Objective Optimization. *IEEE Trans. Veh. Technol.* **2019**, *68*, 5416–5429. [CrossRef]
11. Ibrahim, M.; Bernard, L.; Pichon, L.; Laboure, E.; Razek, A.; Cayol, O.; Ladas, D.; Irving, J. Inductive Charger for Electric Vehicle: Advanced Modeling and Interoperability Analysis. *IEEE Trans. Power Electron.* **2016**, *31*, 8096–8114. [CrossRef]
12. Kishan, D.; Vinod, M.; Harischandrappa, N. Magnetic Coupling Characteristics of Spiral Square-Circular Coupled Coils for Wireless EV Battery Charging System. In Proceedings of the 2020 IEEE 17th India Council International Conference (INDICON)), New Delhi, India, 10–13 December 2020; pp. 1–5.
13. Ahmad, A.; Alam, M.S.; Mohamed, A.A.S. Design and Interoperability Analysis of Quadruple Pad Structure for Electric Vehicle Wireless Charging Application. *IEEE Trans. Transp. Electrif.* **2019**, *5*, 934–945. [CrossRef]
14. Rituraj, G.; Kushwaha, B.K.; Kumar, P. A Unipolar Coil Arrangement Method for Improving the Coupling Coefficient without Ferrite Material in Wireless Power Transfer Systems. *IEEE Trans. Transp. Electrif.* **2020**, *6*, 497–509. [CrossRef]
15. Yang, G.; Song, K.; Sun, Y.; Huang, X.; Li, J.; Guo, Y.; Zhang, H.; Zhang, Q.; Lu, R.; Zhu, C. Interoperability Improvement for Rectangular Pad and DD Pad of Wireless Electric Vehicle Charging System Based on Adaptive Position Adjustment. *IEEE Trans. Ind. Appl.* **2021**, *57*, 2613–2624. [CrossRef]
16. Chen, S.; Xiao, J.; Chen, Q.; Wu, X.; Gong, W.; Wang, X. Research on Interoperability of Coupling Mechanism for Wireless Power Transfer Systems. *Electr. Eng.* **2023**, *105*, 565–573. [CrossRef]
17. Yadav, A.; Bera, T. kanti A Novel, Honeycomb-Magnetic Coupler for WPT in EVs: 3D-Computational Modeling and Validation. *Arab. J. Sci. Eng.* **2024**, *49*, 17001–17021. [CrossRef]
18. Garrofy, I.; Roitman, A.; Nikulshin, Y.; Wolfus, S. Vertical Receiver Coils for Improved Energy Transfer Efficiency in Dynamic Wireless Charging of Electric Vehicles. *Appl. Sci.* **2025**, *15*, 3706. [CrossRef]

19. Khalid, H.; Mekhilef, S.; Mubin, M.; Seyedmahmoudian, M.; Stojcevski, A.; Darvish, P.; Zahid Erel, M.; Alshammari, O.; Jerbi, H. Design and Analysis of Ferrite Less Magnetic Coupler With Improved Dynamic Performance Characteristics for EV Applications. *IEEE J. Emerg. Sel. Top. Power Electron.* **2025**, *13*, 1316–1329. [CrossRef]
20. Li, H.; Wang, K.; Huang, L.; Li, J.; Yang, X. Coil Structure Optimization Method for Improving Coefficient of Wireless Power Transfer. In Proceedings of the 2015 IEEE Applied Power Electronics Conference and Exposition (APEC), Charlotte, NC, USA, 15–19 March 2015; pp. 2518–2521.
21. Moon, S.C.; Moon, G.W. Wireless Power Transfer System with an Asymmetric Four-Coil Resonator for Electric Vehicle Battery Chargers. *IEEE Trans. Power Electron.* **2016**, *31*, 6844–6854. [CrossRef]
22. Tran, D.H.; Vu, V.B.; Choi, W. Design of a High-Efficiency Wireless Power Transfer System with Intermediate Coils for the On-Board Chargers of Electric Vehicles. *IEEE Trans. Power Electron.* **2018**, *33*, 175–187. [CrossRef]
23. Li, W.; Lu, J.; Zhu, G.; Zhang, W.; Jiang, J. Design and Research of a Double-Sided Flux Coupler in Inductive Power Transfer System. In Proceedings of the InIECON 2016-42nd Annual Conference of the IEEE Industrial Electronics Society, Florence, Italy, 24–27 October 2016; pp. 6033–6037.
24. *SAE J2954*; Wireless Power Transfer for Light-Duty Plug-in/Electric Vehicles and Alignment Methodology. SAE Standard: Warrendale, PA, USA, 2024. [CrossRef]
25. Prasad, K.K.; Agarwal, V. Design Recommendations Considering Charging Pads' Self-Inductance Variation With LCC-S and LCC-LCC Compensation Based IPT Chargers in Low Clearance EVs. *IEEE Trans. Transp. Electrif.* **2024**, *10*, 1758–1770. [CrossRef]
26. Farghly, A.; Mohamed, A.; Awad, H.; Abdelfatah, S.; Alharbi, M.A.; Alqarni, M.; Ali Abdelrazik, S. A Comprehensive Review of Wireless Power Transfer Techniques for Electric Vehicle Charging. *IEEE Access* **2025**, *13*, 199683–199718. [CrossRef]
27. Bouanou, T.; El Fadil, H.; Abbade, H. Wireless Charging for Electric Vehicles: A Comprehensive Review of Technologies, Challenges, and Solutions. *J. Power Sources* **2025**, *660*, 238501. [CrossRef]
28. Shrestha, N.; Williamson, S. Hybrid Compensation Network for Misalignment-Tolerant Constant Current/Constant Voltage Charging for Wireless Power Transfer System. In Proceedings of the 2024 IEEE Transportation Electrification Conference and Expo, ITEC 2024, Chicago, IL, USA, 19–21 June 2024.
29. Tian, S.; Wang, H.; Zhang, H. A Hybrid Compensation Topology with Constant Voltage and Constant Current for EV Bidirectional Wireless Charging. In *Proceedings of the IEEE International Conference on Industrial Technology*; Institute of Electrical and Electronics Engineers Inc.: Piscataway, NJ, USA, 2025.
30. Bagchi, A.C.; Kamineni, A.; Zane, R.A.; Carlson, R. Review and Comparative Analysis of Topologies and Control Methods in Dynamic Wireless Charging of Electric Vehicles. *IEEE J. Emerg. Sel. Top. Power Electron.* **2021**, *9*, 4947–4962. [CrossRef]




https://doi.org/10.3390/en19051258